International Journal of Biological Macromolecules 233 (2023) 123273

Contents lists available at ScienceDirect

International Journal of Biological Macromolecules

journal homepage: www.elsevier.com/locate/ijbiomac

Preparation of alginate coated Pt nanoparticle for radiosensitization of breast cancer tumor

Hamid Rashidzadeh [a,b], Farzad Seidi [a,*], Mohammadreza Ghaffarlou [c], Marziyeh Salehiabar [d], Jalil Charmi [d], Kadir Yaray [e], Hamed Nosrati [d,**], Yavuz Nuri Ertas [d,f,***]

[a] Jiangsu Co-Innovation Center of Efficient Processing and Utilization of Forest Resources and International Innovation Center for Forest Chemicals and Materials, Nanjing Forestry University, Nanjing 210037, China
[b] Zanjan Pharmaceutical Biotechnology Research Center, Zanjan University of Medical Sciences, Zanjan, Iran
[c] Hacettepe University, Department of Chemistry, Beytepe, Ankara 06800, Turkey
[d] ERNAM—Nanotechnology Research and Application Center, Erciyes University, Kayseri 38039, Turkey
[e] Department of Radiation Oncology, Faculty of Medicine, Erciyes University, Kayseri, Turkey
[f] Department of Biomedical Engineering, Erciyes University, Kayseri 38039, Turkey

ARTICLE INFO

Keywords:
Radiotherapy
Radiosensitizer
Platinum nanoparticle
Alginate
High Z

ABSTRACT

Noble metals as high atomic number elements can localize X-ray radiation within tumor cells by exploiting different mechanisms. Here, alginate (Alg)-coated platinum nanoparticles (Pt@Alg) were synthesized, characterized, and implemented as a radiosensitizer to enhance X-ray therapeutic efficacy in breast cancer *in vitro* and *in vivo*. Alg not only improves the biocompatibility of the radioenhancer, but also stabilizes the nanoparticles. Pt@Alg was studied by different characterization methods including DLS, STEM, Fe-SEM, XRD, XPS, FT-IR and UV–Vis spectrophotometry. The nanosystem provided a higher level of intracellular ROS in malignant cells and enhanced cancer cell death under X-Ray irradiation. Clonogenic assay also demonstrated the radiosensitizing properties of the nanosystem, *in vitro*. *In vivo* result show tumor growth restraining properties of the nanosystem when it was administrated along with X-Ray irradiation. Histopathology results confirmed the impact of nanosystem and X-ray co-treatment, as well. Altogether, the importance of radiosensitizers for improving radiotherapy outcomes was highlighted.

1. Introduction

According to WHO (World Health Organization) report, breast cancer is the 5th known reason for cancer-related death and the most frequent cancer type in women [1,2]. The malignancy burden is undeniable in women and the number of new cases are estimated 2.7 million by 2030 with 0.87 million dead. This most common non-skin cancer and the leading reason responsible for premature death in US, can be screened regularly with mammography and MRI and as a result, decline 40 % of death [3]. Various modifiable and non-modifiable factors such as family history, obesity, reproductive and hormonal status are involved in breast cancer incident [4].

Despite treatment advances, mortality rate in advanced-stages remain high. Although, different conventional treatment options are available depending on the stage of disease including surgery, radiotherapy, adjuvant/ neoadjuvant systemic therapy (chemotherapy, targeted and endocrine treatment). Metastatic cancers are subjected to supportive care and symptomatic treatment along with other traditional treatments such as radiotherapy [5]. This modality is highly effective in solid tumor and useful in >50 % of patients in which adjuvant radiotherapy improves overall survival and decrease recurrence risk by 66.7 % in advanced stages. The underlying mechanism of ionizing radiation effectiveness is either direct damage to macromolecules, or indirect generation of ROS (by water hydrolysis) to acquire cell death through various molecular pathways [6].

Regardless of expended efforts this modality is accompanied by adverse effects that are unbearable and necessitate special attention. While precise delivery of ionizing radiation to tumor site attenuate near-

* Correspondence to: F. Seidi, Nanjing Forestry University, Nanjing, 210037, China.
** Corresponding author.
*** Correspondence to: Y.N. Ertas, ERNAM—Nanotechnology Research and Application Center, Erciyes University, Kayseri 38039, Turkey.
E-mail addresses: f_seidi@njfu.edu.cn (F. Seidi), nosrati.hamed2020@gmail.com (H. Nosrati), yavuzertas@erciyes.edu.tr (Y.N. Ertas).

https://doi.org/10.1016/j.ijbiomac.2023.123273
Received 28 October 2022; Received in revised form 3 January 2023; Accepted 11 January 2023
Available online 14 January 2023

by healthy tissue damage, there is a limitation for radiation dose especially in case of radio-resistant tumors and near-by organs at risk [7]. To conquer drawbacks of this therapeutic modality in breast cancer patients such as cardiovascular toxicity and skin reaction (which is corresponding to radiation dose increase), therapeutic agents were developed to sensitize tumor cells to radiation and improve treatment outcome while reducing the radiation dose [8,9]. This so called 'radiosensitizers' are effective through interaction with ionizing radiation and thus producing reactive species which ultimately damage biological macromolecules, leading to cell death [10].

A powerful tool for developing effective radiosensitizers is nanomedicine, especially inorganic nanomaterials. One the one hand, conventional radio sensitizer face poor bio availability and tumor selectivity [11]. On the other hand, nanomaterials possess special intrinsic properties such as passive targeting and enhanced permeation and retention (EPR) effect and can overcome these limitations (owing to their special properties such as size) [12]. High atomic number metals such as Gd, Au and Pt were of great interest so far as they can effectively interact with ionizing radiation and produce enhanced amount of ROS [13]. Change of atomic number cause significant change in X-ray absorption and noble metal nanoparticles are powerful tools for X-ray energy absorption and cause cell sensitivity through biochemical and physical sensitizing mechanisms. Noble metal nanoparticle are proved to accumulate in tumor site and improve RT therapeutic outcome while being inert chemically and ideally non-toxic to normal cells. Porous platinum nanoparticle for simultaneous radiation energy deposition and hypoxia attenuation was designed by Li et al. Effective RT therapeutic enhancement was observed as platinum interacted with X-ray and playing an enzymatic role in converting excessive H_2O_2 produced by rapidly proliferating cancer cells [14]. Platinum nanoparticles possess their own antitumor properties and can efficiently kill upon laser irradiation while being non-toxic at therapeutic concentrations. Importantly, Pt nanoparticles could beat heterogeneous stemness and chemoresistance of hepatocellular carcinoma by cell cycle and DNA damage gene modulation. When Pt nanoparticles coated with peptide, significant anticancer properties was observed over liver cancer cells, more than that of cisplatin [15].

The noble metal nanoparticle can be modified easily by functionalizing with biocompatible polymers. Alginate (Alg) as a natural polymer was chosen for functional surface modification of our proposed platinum nanoparticles. Biodegradability, flexibility, and biocompatibility of Alg are the advantages of this polymer that is combined with nano-scale pros of such particles to achieve more sensitization in cancer cells. Herein, Alg-coated platinum nanoparticles (Pt@Alg) as a noble metal-biopolymer hybrid was proposed to enhance radiation energy deposition inside tumor by interaction with X-ray and emitting electrons that further produce ROS more and more.

2. Materials and methods

Sodium alginate (Appearance: Solid, white to beige and faint brown to light brown; Loss of drying: ≤ 15.5 %; Viscosity: 5–40 cps; pH: 5–8) was purchased from ISOLAB (Turkey). Chloroplatinic acid hexahydrate ($H_2PtCl_6{\cdot}6H_2O$) (powder and chunks, ≥ 37.5 % Pt basis) was purchased from Sigma Aldrich Inc. Sodium borohydride ($NaBH_4$) (powder, ≥98.0 %) was purchased from Sigma Aldrich Inc. (St. Louis, Missouri, United States). RMPI 1640 (w: L-Glutamine, w: 25 mM HEPES, w: 2.2 g/L $NaHCO_3$), DPBS (w/o: Calcium, w/o: Magnesium), and Trypsin/EDTA (0.25 % / 0.02 % in PBS, w/o: Ca, and Mg, W: Phenol red) were purchased from PAN BIOTECH (Aidenbach, Germany). Pen-Strep Solution X10 (Penicilin: 100,000 units/mL; Streptomycin: 100 mg/mL) was purchased from Sartorius (Göttingen, Germany). Fetal Bovine Serum (FBS), European Grade was purchased from BI Biological industries (0.1 μm Membrane Filtered, Mycoplasma Tested, Virus Screened) (Israel). MTT (3-(4,5-Dimethylthiazol-2-yl)-2,5-Diphenyltetrazolium Bromide) was purchased from Invitrogen (Waltham, Massachusetts, United States). Calcein-AM (Solid ≥90 % (HPLC), Calbiochem®), Propidium iodide (PI) (Powder ≥94 % (HPLC)), Hematoxylin (powder, Quality level: 200), Eosin (Powder, Quality level: 100, 75 % (HPLC)) and 2′,7′-Dichlorofluorescin Diacetate (DCFH-DA) (crystalline solid, ≥94 % (HPLC), Calbiochem®) were purchased from Sigma Aldrich Inc. (St. Louis, Missouri, United States).

2.1. Synthesis of Alg-coated Pt nanoparticle

Pt@Alg was prepared by mixing Alg (100 g) in distilled water (30 cc) at 50 °C to acquire complete dissolution. This was followed by the addition of platinum solution (160 μL, 1 M) and then 400 μL of $NaBH_4$ (10 mg/mL), as a reducing agent to trap platinum inside spaces of Alg polymer. The solution was dialyzed against distilled water to purify the nanohybrid.

2.2. Characterization

Confirming the successful synthesis of nanoparticles is necessary before exploiting them for *in vivo/ in vitro* experiments. Scanning transmission electron microscope (STEM) and Field emission scanning electron microscopy (FeSEM) (Zeiss Gemini 500, Germany) were utilized to determine morphology and size of nanoparticles. Dynamic light scattering (DLS, by nanosizer) was utilized to determine size and surface zeta potential (Malvern Instruments, Worcestershire, UK, ZEN 3600 model Nano ZS). Fourier-transform infrared spectroscopy (FTIR) (FTIR; SHIMADZU, Model IRTRACER-100) was used to document the FTIR spectra of samples. UV–Vis spectrophotometry (UV–Vis; Perkin Elmer, lambda 25) also determined the optical properties of Pt@Alg. Energy-dispersive X-ray spectroscopy (EDX) (A Supra 35VP Leo EDX instrument, Germany) analysis was used to investigate elemental composition and distribution. X-ray diffraction (XRD) pattern was determined by Powder X-ray diffractometer system (PANalytical X'Pert Powder Diffractometer, United Kingdom) using Cu Kα radiation (k = 1.542 A). X-ray photoelectron spectroscopy (XPS) was performed using a monochromatized Al Kα X-ray source (Thermo Scientific, USA).

2.3. In vitro assays

2.3.1. Biosafety assays of Pt@Alg

Preclinical studies are necessary to demonstrate the biocompatibility of synthesized nanosystems as all the therapeutic agents come to contact with blood components and tissues, eventually. As a matter of fact, hemoglobin is released upon red blood cells (RBC) damage and is exploited as an indicator of RBC incompatibility. Hemocompatibility of nanomaterial was assayed before further investigations according to previous protocols [12].

Normal cell cytotoxicity of Pt@Alg on Human umbilical vein endothelial cells (HUVEC) cell line was conducted as a complementary test for nanomaterials biosafety assessment. After cells were seeded in a 96-well plate (5×10^3 cells in each well) and incubated for a day, new cell culture medium containing Pt@Alg was substituted. The cells were incubated in contact with different concentrations of Pt@Alg (50, 100, 200, and 400 μg/mL) for 5 h. Next, cells were incubated with fresh cell culture medium for another 24 h. MTT solution (5 mg/mL, 20 μL) was added to each well and incubated for 4 h. After removing culture media, DMSO was added to dissolve formazan (100 μL was added to each well). The experiment was repeated 5 times and optical density of dissolved formazan crystals were assessed at λ = 570/640 nm, read by microplate reader (SYNERGY/HTX, S1LFA).

2.3.2. Cell cytotoxicity study on 4T1 cells

MTT assay was conducted to determine cytotoxicity effect of Pt@Alg nanoparticles on 4 T1 cell line (Mouse breast carcinoma cell line). The influence of X-ray irradiation on cell viability was investigated in this step. The seeded 4 T1 cells in the 96-well plates (5×10^3 cells per well)

were treated with nanoparticles in 50, 100, 200, and 400 μg/mL concentrations. Followed by 5 h of incubation, the nanoparticle-treated medium was removed and cells were cleansed using PBS and fresh cell culture was added. The cells were exposed to X-ray (4 Gy, 6MV) and MTT assay followed after 24 h incubation. MTT assay was utilized to evaluate the radiosensitizing and anti-cancer properties of Pt@Alg and groups were compared with the control group.

2.3.3. Colony forming assay

As a common cell biology assessment, a clonogenic assay was utilized to investigate the radiosensitivity of 4 T1 cells. After treatment of cells with nanoparticles for 5 h and exposure to X-ray irradiation, the cells were incubated for further 9 days, then the number of developed colonies and seeded cells were counted and the survival fraction was calculated [16]. The biological response of cells was represented as a survival fraction and compared with the control group (non-treated and non- irradiated).

2.3.4. Live and dead cell assay

Further, calcein acetoxymethyl ester/propidium iodide (calcein AM/PI) cell staining was utilized to distinguish alive and dead cells from each other by fluorescence imaging. Calcein AM and PI fluorescent dyes emit green and red light, representing alive and dead cells upon excitation, respectively. 4 T1 cell line were exposed to X-ray radiation either alone or in combination with Pt@Alg nanoparticle. Then, cells were exposed with ionizing radiation. Groups were as followed: Control, X-ray, Pt@Alg + X-ray, Pt@Alg. Firstly, 4 T1 cells were seeded in a 96-well plate and incubated for 24 h. The cells were exposed to Pt@Alg nanoparticle in a standard condition for 5 h. Cells were subjected to staining with PI and calcein AM at 4 μM and 3 μM, respectively, 24 h after treatment. Images of alive and dead cells obtained from fluorescence microscope, were merged and viable cell count was considered as a criterion for assessment of Pt@Alg radiosensitizing effect.

2.3.5. Intracellular ROS generation

The generation of intracellular ROS by DCFH-DA, which can be oxidized to a highly fluorescent DCF by ROSs. 4 T1 cells were incubated at 37 °C for 24 h on 96 well plates at density of 5×10^3 cells. The cells were exposed to Pt@Alg nanoparticles in a standard condition for 5 h. After removing the particle dispersion, the cells were treated for 1 h with 15 μM DCFH-DA. Then those were irradiated with X-ray (4 Gy, 6MV). After washing the cells with PBS, the images were taken by fluorescence microscopy [16].

2.4. In vivo assays

2.4.1. Anti-tumor effect

All animals were maintained in a 12-hour light/12-hour dark normal cycle, fed normally, and had access to food and water. Anti-tumor properties of Pt@Alg was demonstrated in 4 T1-tumor bearing mouse either in the presence or absence of X-ray ionizing radiation. For this purpose, 4 T1 cells were inoculated by subcutaneous injection (1×10^6) into the right flank of female BALB/c mice. Tumor dimensions were measured by digital caliper and the volume was calculated according to formula: $V = 0.5 \times L \times W^2$. When tumor volume reached 300 mm^3, treatment was initiated, and animals were randomly divided into four groups in every group consisting of 5 mice. Then tumor treatment was initiated with Pt@Alg nanoparticle with/or X-ray radiotherapy. Groups of mice measured for tumor volume and body weight are as followed: 1) Control group treated with PBS, 2) X-ray- irradiation, 3) Pt@Alg, 4) Pt@Alg + X-ray. Tumor size at different days were represented relative to the initial volume assessed at day 0 (V/V0) and Pt@Alg nanoparticle was injected into the tail vein. All animals were monitored during the experim for body weight, and tumor volume.

2.4.2. Histopathology

On day 21th, mice were euthanized and breast tumors was resected and sectioned for tumor histopathological investigation after different treatments. After treatment with Pt@Alg and/or X-ray, tumors was collected, fixed in 4 % paraformaldehyde. Then, paraffin-embedded murine breast tumor tissue were cut into slice and visualized for histological features after staining with hematoxylin and eosin (H&E).

2.5. Statistical analysis

All data was expressed as mean ± SD and one-way analysis of variance (ANOVA) was employed for comparing groups.

3. Results and discussion

3.1. Preparation of Alg-coated platinum nanoparticle

An environment-friendly and facile synthesis was designed to acquire Pt@Alg nanoparticles in aqueous media at 50 °C. Accordingly, platinum salt was added to the Alg solution and reduced by $NaBH_4$ upon interaction with negative functional groups and trapping in free spaces of Alg. Once platinum nanoparticles were formed, dialysis was exploited to obtain purified nanoparticles and remove unreacted ions. Alg polymer plays a crucial role in the biocompatibility, water solubility, and physical stability enhancement of platinum nanoparticles. Moreover, Alg can interact with cations instantly and produce inotropic Alg hydrogels which is used for decades for *in vivo* biomedical applications [17]. Herein, we utilized the natural polysaccharide to entrap Pt ions and then produce Alg-coated Pt nanoparticles. Further, the prepared Pt@Alg was investigated to assure accurate synthesis by different characterization methods.

3.2. Characterization

After obtaining purified Pt@Alg, several assays were conducted to assess important characteristics of Pt@Alg and confirm the success of synthesis. The size and morphology of nanoparticles were investigated with STEM and FeSEM and corresponding images are displayed in Fig. 1a and b, respectively. Spherical and monodispersed Pt@Alg nanoparticle was observed in both STEM and FeSEM images. Results show that nanoparticles were homogenously dispersed. Fig. 1c represents hydrodynamic size distribution of nanoparticles assessed by DLS technique which showed a mean diameter of 99.09 nm and a polydispersity index of 0.208 which is acceptable. The difference between the size measured by TEM and DLS is Alg swelling in contact with water, considering the STEM images depict the dried sample and DLS measured the size when nanoparticles were dispersed in an aqueous solution [18,19]. It should be mentioned that this difference (about 5-folds) is also acceptable. The size and surface charge of nanoparticles is the pivotal factors affecting *in vivo* and *in vitro* performance of nanosystems and should be investigated prior to any application in biological environments. Then, the zeta potential of nanoparticles was measured which is a key factor in its colloidal stability and interaction with biological components. Similar and larger surface charge act in favor of higher colloidal stability as nanoparticles repel each other and suspend in the media. Hence, zeta potential plays a major role in nanosystem interaction with cell layers, plasma and blood cells. As they have a negative charge, nanoparticles possessing a negative surface charge will have almost no interaction with blood components and provide higher circulation time. Here, the zeta potential of Pt@Alg nanoparticles was determined as −35.4 mV, indicating high stability of the nanosystem (Fig. 1d).

To confirm the elemental composition of Pt@Alg, EDX was utilized. Elemental mapping images are displayed in Fig. 1e, confirming the presence of platinum (Pt), carbon(C), and oxygen (O) in the synthesized nanosystem and their uniform distribution. Further, XPS analysis was

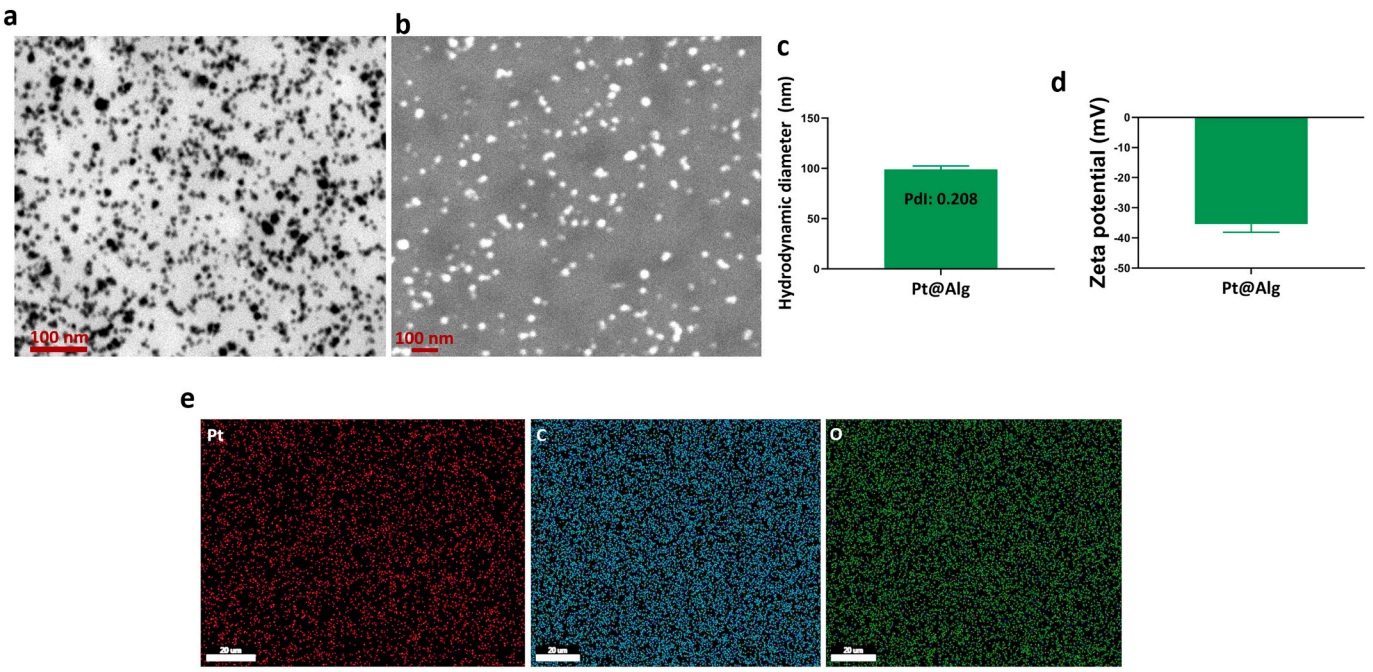

Fig. 1. a) STEM and b) SEM images of Pt@Alg nanoparticles. c) Mean hydrodynamic diameter and d) zeta potential of as-synthesized nanoparticles measured by DLS. e) EDX elemental mapping of Pt@Alg.

conducted (Fig. 2a) to measure elemental composition of Pt@Alg. Na, O, C and Pt are detected elements in XPS spectrum. High-resolution C 1 s core levels and Pt 4f were shown in Fig. 2b and c, respectively. Alg is mainly composed of C and O elements which are well-represented in images and the corresponding XPS peaks are totally in accordance with previous studies [20]. The same spectra for Pt were detected in another study at $Pt4f_{5/2}$ and $Pt4f_{7/2}$ with energy binding of 72.6 and 75.6 eV which indicates that nanoparticles are composed of zero-valent Pt [21]. The elements detected by the XPS survey spectrum were matched to those mapped in EDS. The presence of all elements was confirmed in a full range survey of the XPS spectrum, indicating successful synthesis of nanoradiosensitizer. XRD was also employed for further confirmation of the Pt@Alg structure (Fig. 2d). Spectrum peaks at $2\theta = 39.8°$, 46.2°, 67.5°, and 81.3° corresponding to (111), (200), (220), and (311) were identical to JCPDS Pt card (No. 04–0802), indicating platinum existence in the nanostructure.

FTIR spectra of Pt@Alg and Alg were displayed in Fig. 2e. Alg peaks are evident at 1027 cm^{-1} representing attributed to C–O–C stretching vibration [22], and asymmetric and symmetric stretching vibration of COO groups were seen at 1597 cm^{-1} and 1408 cm^{-1}. Pt peaks are mostly covered by Alg peaks. Also, a shift at 1606 cm^{-1}1, 1416 cm^{-1} and 1032 cm^{-1} are evident in the Pt@Alg spectrum which is due to Pt interaction with Alg. These are well-supported by previous studies [23,24]. FT-IR spectrum of Pt@Alg represents both characterristic bands of Alg and Pt, and thus indicates successful synthesis of Pt@Alg.

3.3. *In vitro biosafety assays*

3.3.1. *Hemolysis assay*

Pt@Alg was incubated with human RBC and its hemocompatibility was assessed at 50, 100, 200, and 400 μg/mL. Negligible (<2.7 %) hemolysis at the highest concentration tested, implies excellent biosafety, and compatibility as well as ensures its safe intravenous administration (Fig. 3a). This was in line with a recent result of a publication on Pt@BSA, demonstrating good biocompatibility [25]. Deionized water was assumed as a positive control, meaning incompatibility with RBC and PBS caused no hemotoxicity considering the isotonic properties of the solution. Nanosystem safety was indicated despite increasing hemolysis with increasing concentration of Pt@Alg. No demonstrated damage to human RBC, guarantee hemocompatibility of Pt@Alg.

3.3.2. *Healthy cell cytotoxicity*

MTT assay measures the number of metabolically-active cells, indirectly by converting soluble yellow die to insoluble purple crystals by an enzyme in mitochondria called dehydrogenase [26]. Thus the number of viable cells and cytotoxicity of newly- synthesized nanomaterials can be determined [27]. It is urgent to evaluate the cytotoxicity of Pt@Alg against normal cells prior to determining *in vitro/in vivo* radiosensitizing ability. HUVEC normal cell line was exposed to synthesized Pt@Alg at 50, 100, 200, and 400 μg/mL concentrations to assess its cytotoxicity. Results specify good cell viability at all concentrations and no toxic effect was indicated on HUVEC cells, as illustrated in Fig. 3b. By increasing the concentration of Pt@Alg, cell viability decreased but no deleterious effect on cell survival was determined at the maximum concentration tested. Similarly, human breast epithelium (CRL-4010) was treated with Platinum nanoparticles for 24 h and cell viability decreased in parallel with dose elevation. They found that at 200 μg/mL of PtNP cell viability of CRL-4010 reduced by 55 % while in our investigation, 75 % of cell viability was observed at 400 μg/mL of Pt@Alg nanoparticle [28]. This biosafety is obtained probably due to Alg's presence, as a biocompatible polymer which enhances nanosystem safety. Thus, the biocompatibility of Pt@Alg nanosystem was confirmed for preclinical studies at concentrations tested except at 400 μg/mL which low toxicity was demonstrated.

3.4. *In vitro efficacy assays*

3.4.1. *Anti-proliferative and sensitizing effect of Pt@Alg on malignant cell line*

Pt@Alg was assessed for *in vitro* cytotoxicity against murine breast cancer cells, 4T1 cell line. As illustrated in Fig. 3c, Pt@Alg nanoparticle showed concentration-dependent cytotoxicity in which 50 μg/mL showed 86 % cell viability and by increasing concentration to 400 μg/mL, cell viability decreased to 57 %. At the same concentration of Pt@Alg normal cell viability was obtained about 91 % and 72 %, respectively. These results indicate a more pronounced treatment

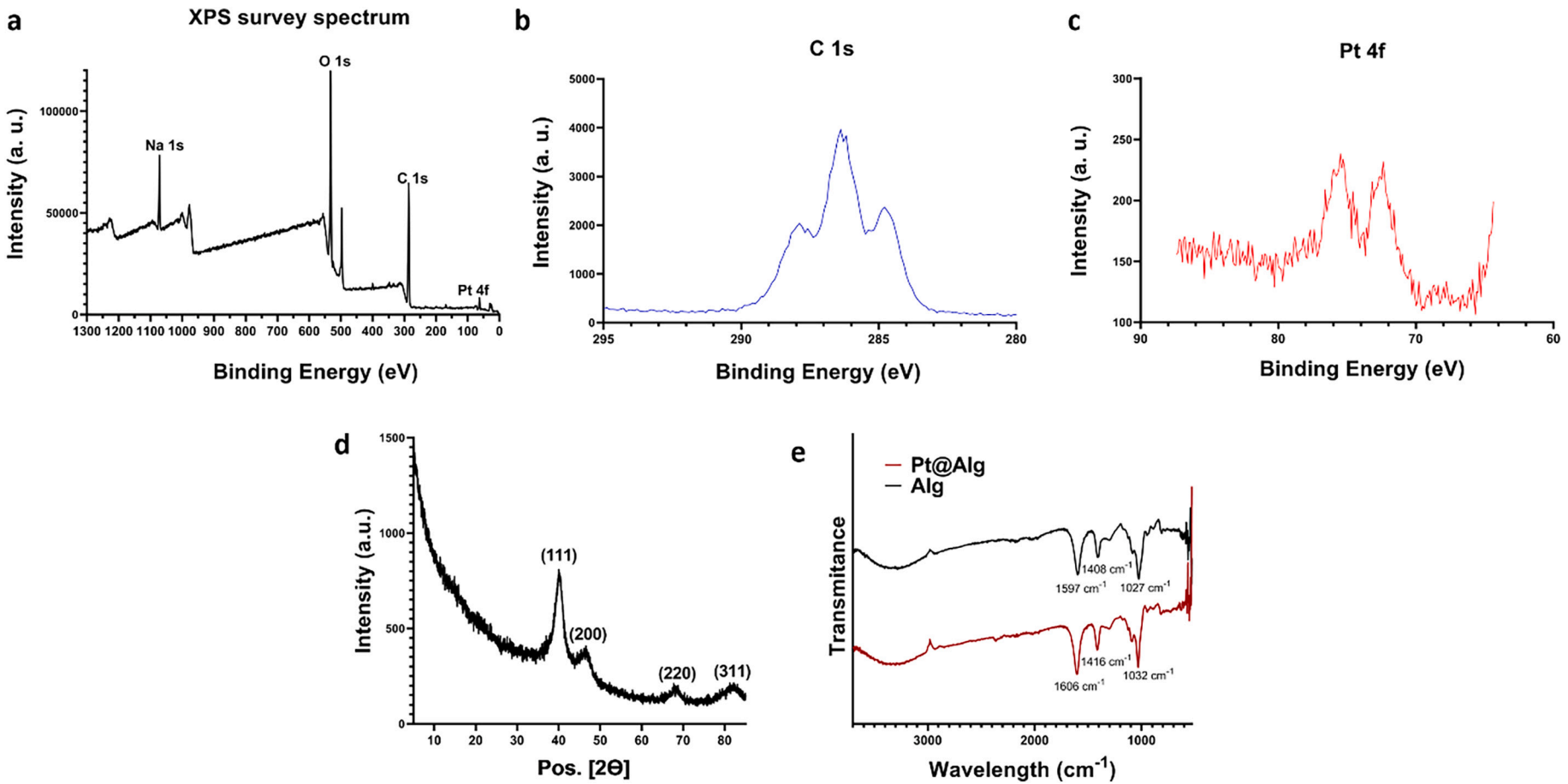

Fig. 2. a) Full range XPS survey spectrum analysis of Pt@Alg. b) High-resolution C 1 s core levels and c) High-resolution Pt 4f core levels. d) XRD spectrum of as- synthesized nanoparticles. e) FTIR spectrum of Pt@Alg nanoparticle and Alg.

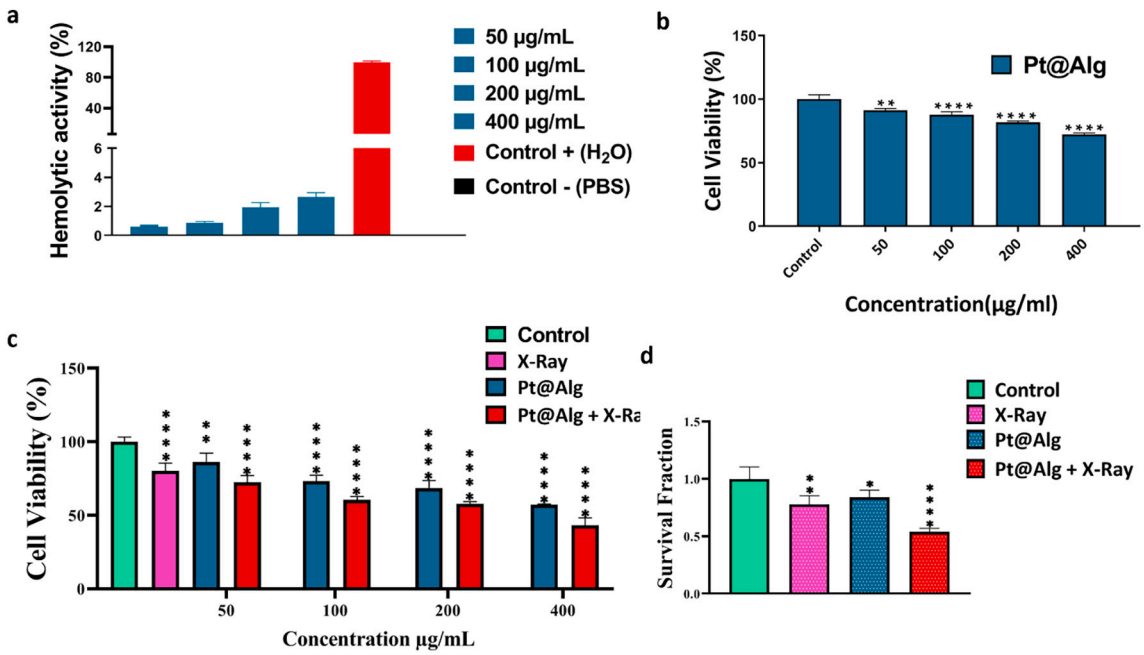

Fig. 3. Biosafety assays and *in vitro* cytotoxicity of Pt@Alg. a) Hemolysis assay of synthesized Pt@Alg, b) Normal cell cytotoxicity. c) Cell viability of 4 T1 cells upon different treatments. d) Survival fraction of colonies formed after treating with different treatment planes. Data = mean ± SD; $^{*}P < 0.05$, $^{**}P < 0.01$, $^{***}P < 0.001$, and $^{****}P < 0.0001$ compared to the control group.

response in 4 T1 cancer cells, compared to HUVEC cells which are more distinguishable at higher concentration of nanoparticles. Thus cell-dependent cytotoxicity was demonstrated which is well supported by previous studies of gold and platinum nanoparticles on MCF-7 and SKBR3 cell lines, respectively [28,29]. Moreover, malignant cells were exposed to X-ray, alone (X-ray group) or in combination with Pt@Alg nanoparticles (at different concentrations) to evaluate the radiosensitizing effect of Pt@Alg. As shown in Fig. 3c, when irradiation accompanied by nanoparticle treatment, it had a good impact on reducing cell viability, at all concentrations tested compared with the X-ray group (4 Gy). When cells were irradiated with X-ray, the viable cell population reduced significantly in comparison with the control group. Despite X-ray's usefulness in eliminating cancer cells, it is far from perfect in suppressing and controlling cancer cells. By increasing Pt@Alg nanoparticle concentration, more significant cytotoxicity was acquired which is due to the radiosensitizing effect of Pt@Alg upon X-ray irradiation. Thus, the radiosensitizing effect of Pt@Alg was indicated as nanosystem improved dead cell population under X-ray irradiation and thus enhanced radiotherapy efficacy. Our data is well supported with *in vitro* therapeutic X-ray efficacy assessed in a study demonstrating porous PtNP impact on enhancing the anti-cancer effect of irradiation. Similarly, porous PtNP at 50 µg/mL and 5 Gy induced cell death by approximately 55 % [30]. Thus the pivotal role of platinum nanoparticle as a noble metal with high-Z is underlined in enhancing the therapeutic efficacy of X-ray on malignant cell line and sensitizing them to radiation while Pt@Alg induce cell death selectively in normal cell line by themselves.

3.4.2. Clonogenic assay

To evaluate cell growth inhibition (as a criterion for cell cytotoxicity) induced by different treatments, *in vitro* colony-forming assay was conducted. In this context, the 4 T1 cell line was incubated with Pt@Alg and/or exposed to X-ray. The survival fraction was calculated and depicted in Fig. 3d. The colony formation capability of simultaneously-treated cells with X-ray and Pt@Alg was significantly attenuated in comparison and evidently less than that of the X-ray or Pt@Alg group. Significant cell growth arrest and reduced colony forming ability of Pt@Alg + X-ray group point to the radiosensitizing effect of as-synthesized nanoparticles which benefit from the fact that radiosensitizers potentiate ROS generation upon radiation. Similar results were noted in the clonogenic assay of gold nanospikes and demonstrated the radiosensitizing effect of this high-Z-based nanoparticle on the survival fraction of the X-ray irradiated-group. Survival fraction reduced to 51 % which supports our data on survival fraction of Pt@Alg + X-ray group [31].

3.4.3. Live and dead cells assay

For further cancer cell cytotoxicity investigations of Pt@Alg, alive/dead cell staining was employed to distinguish dead cells from alive ones after different treatments. Calcein AM and PI emitted green and red fluorescent light representing live and dead cells, respectively. The radiosensitizing potential of Pt@Alg upon X-ray irradiation was determined by the number of dead and viable cells observed. Fig. 4a illustrates dead/live malignant cells, after administration of PBS (Control, untreated), X-ray, Pt@Alg and X-ray + Pt@Alg. Merged pictures in the last raw can be compared easily. More viable cells are observed in the control group, corresponding to green light in the fluorescent image and the number of viable cancer cells are the least in the case of X-ray and radiosensitizer co-treatment group. As evidenced in Fig. 4a, in comparison to other groups X-ray + Pt@Alg group manifested the most number of dead cells, indicating potentiation of X-ray cell-death induction in 4 T1 cells by radiosensitizer. This highest number of dead cell in X-ray + Pt @Alg indicates the strong radiosensitizing effect of Pt @Alg and emphasize its role in sensitizing malignant cells to radiotherapy (4 Gy). This is owing to Pt presence which is a high atomic noble atom, enhancing the mortality rate of irradiated cells considerably *via* ROS production. The next section investigates ROS generating properties of Pt@Alg.

3.4.4. Intracellular ROS generation

ROS has a fundamental role in cell damage induction upon X-ray irradiation and consequently cause cell death [32]. DCFH-DA was used to evaluate the amount of ROS produced inside 4 T1 cells through treatment with radiation and/or nanoparticle. As shown in Fig. 4b fluorescent intensity increased slightly in the X-ray and Pt@Alg group which is well-supported by data from a study on ROS production inside

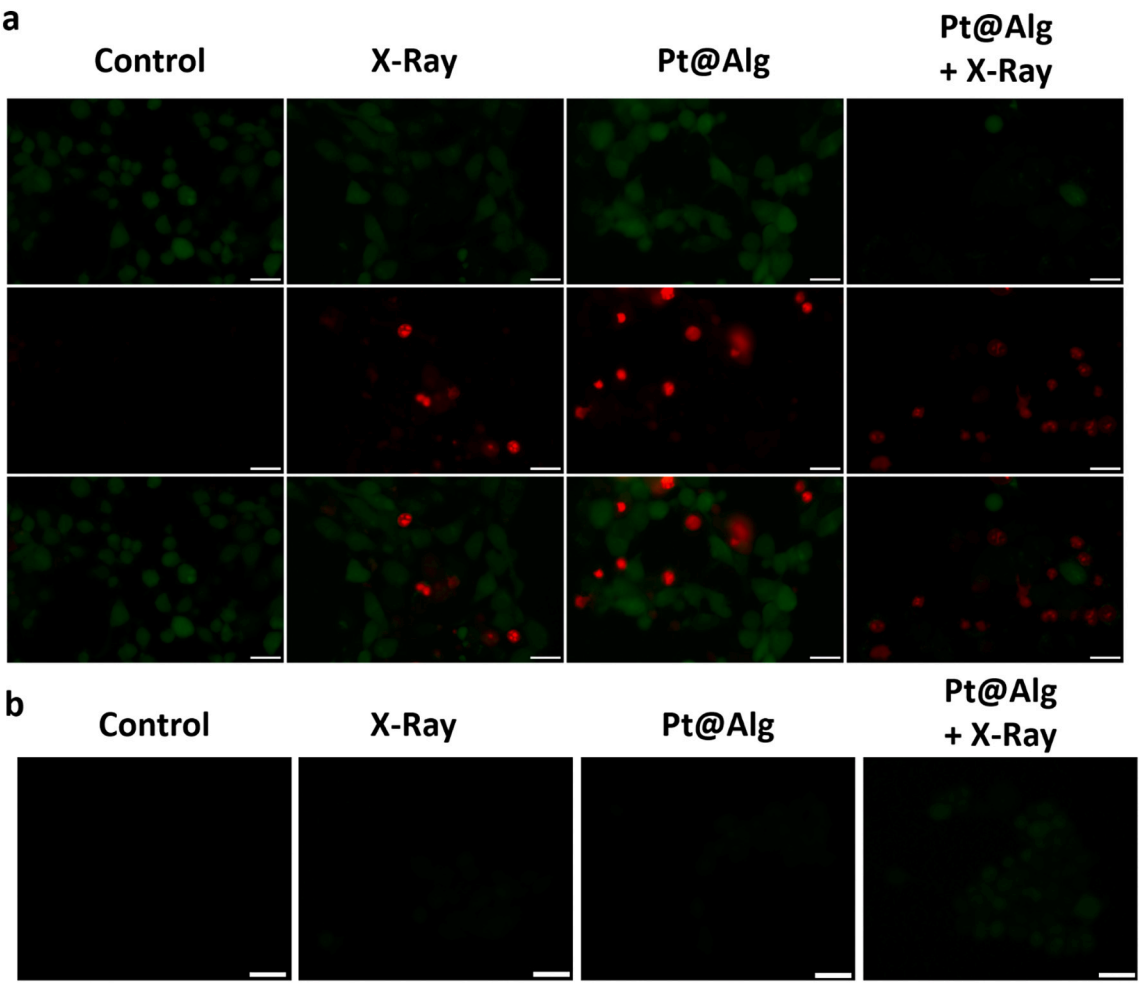

Fig. 4. a) Calcein AM/PI co-stained 4 T1 cells for evaluating cytotoxicity of Pt@Alg with/without radiotherapy. b) Intra-cellular ROS generation upon radiotherapy with/without incubation with Pt@Alg. Scale bar: 20 μm.

melanoma cells undergoing the treatment with Pt NPs [33]. The control group demonstrated no light emittance and also no intracellular ROS generation. Compared to the control group, a slight brightness increase in Pt@Alg group. The most striking result obtained from this experiment was the radiosensitizing effect of Pt@Alg nanoparticle as fluorescent intensity and intracellular ROS level was detected the most in malignant cells treated concurrently with X-ray + Pt@Alg. These data correlate favorably well with Jiang et al. study on ROS level produced inside HeLa cells which amplified by MoSe2 nanoflower radiosensitizing effect in X-ray presence. [34]. Higher oxidation level of DCFH-DA and consequently enhanced fluorescent intensity observed in the X-ray + Pt@Alg group indicates an elevated amount of ROS presence inside the cells and as a result extensive cell damage upon X-ray irradiation (amount of generated ROS: Pt@Alg + X-ray > X-ray Pt@Alg > Control). Based on synergistic ROS generation observed in Pt@Alg + X-ray group, it can be concluded that Alg-coated Pt nanoparticle is a promising tool for more sensitization of cancer cells.

3.4.5. *Anti-tumor therapeutic efficacy*

Radiotherapy is known as a beneficial modality with an affirmative role in minimizing the growth of solid tumors, shrinking breast tumor, as well as killing breast cancer cells [35]. Besides therapeutic efficacy, radiotherapy of breast tumors is associated with drawbacks including nearby healthy tissue damage, cardiotoxicity, and incomplete tumor ablation [36,37]. *In vivo* complementary tests were necessary to confirm *in vitro* obtained results in this study, demonstrating synergistic cancer cell elimination in concurrent employment of X-ray radiation and as-synthesized radiosensitizer. 4 T1 tumor-bearing mice were investigated for tumor volume during the experiment when treated with intravenous injection of PBS, Pt@Alg, and/or exposure with X-ray (4 Gy). Treatment was initiated after tumors reached a certain volume (~ 300 mm^3) and divided randomly into four groups. Following single-dose tumor treatment and radiation therapy on day 0, tumor volume and body weight of tumor-bearing mice were recorded precisely for 20 days. Figs. 5a and b, illustrate the tumor volume change curve and body weight during experiment time, respectively. The tumor volume of the non-treated and non-irradiated group (Control) increased continuously. In comparison to the control, tumor growth of other mice was inhibited to different extents. The experiment showed tumor growth suppression in the X-ray group (in comparison to control and Pt@Alg) but the growth inhibition was the most significant when mice were treated simultaneously with radiation and nanosystem (Pt@Alg + X-ray group). In brief, co-administration of Pt@Alg nanoparticle with X-ray irradiation (4 Gy) showed the best therapeutic effect against tumor growth which signifies accentuated tumor tissue damage induced by radio-sensitizer. The same tumor growth suppression efficacy was observed in a study on 4 T1-bearing mouse exposed to X-ray (10 Gy) with PEG-modified bismuth gadolinium oxide nanoparticle as metal-based radiosensitizer [38]. In another study, as indicated by Zhang et al., the best *in vivo* therapeutic effect was demonstrated in tumor-bearing mice treated with BiPt-PFA + X-ray [39] (bismuth mesoporous-platinum nanodot- polyethylene glycol-folic acid).

The body weight change curve of each group was monitored and displayed in Fig. 5b for each group as an indicator of mouse health

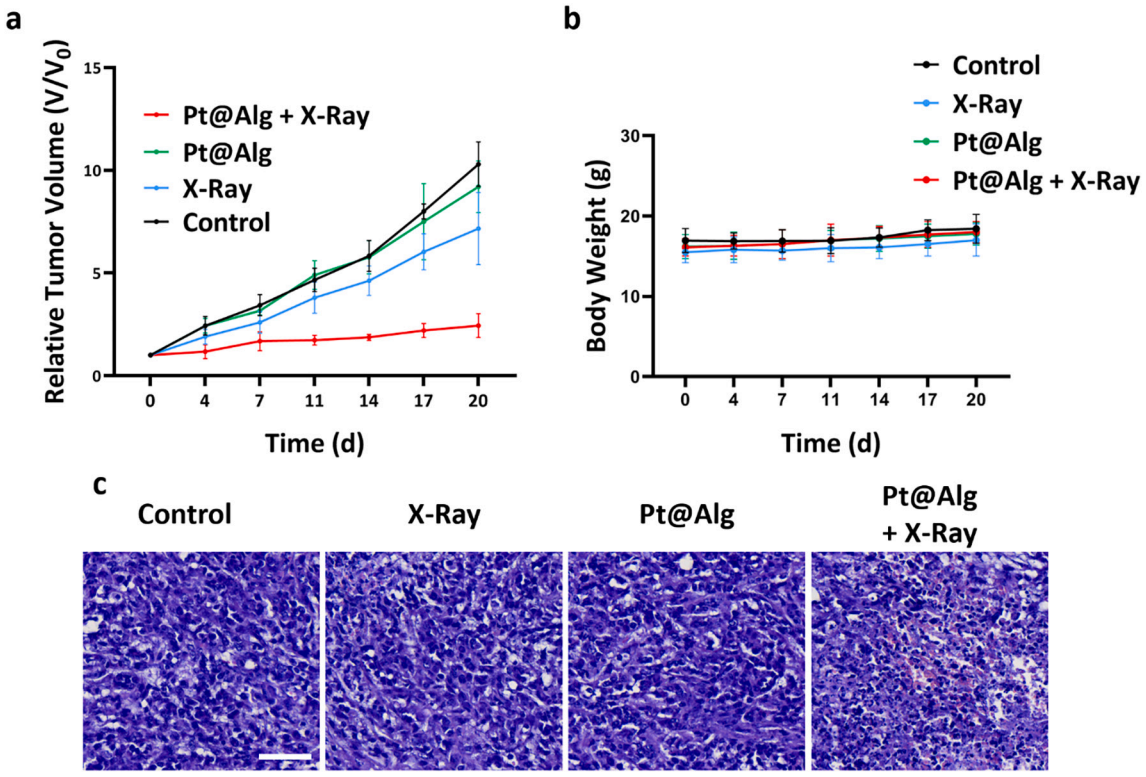

Fig. 5. a) *In vivo* anti-tumor efficacy of nanoradiosensitizer with/without radiotherapy (Relative tumor volumes). b) Monitoring body weight during 20 days of experiment. c) Histological section of extracted tumors on day 21. Scale bar: 50 μm.

status. On average, animals in all groups experienced a minor weight fluctuation during the experiment. As a result, it emphasize the safety of employed radio-sensitizer.

3.4.6. Histopathology analysis

After day 20th, mice were euthanized and tumors were extracted followed by sectioning and H&E staining. As illustrated in Fig. 5c, the untreated tumor tissue section depicted that the nuclei are close to each other. Meanwhile, shadow areas and cell debris were observed in the Pt@Alg + X-ray group which was mainly caused by cell death induced by co-administration of Pt@Alg + X-ray. This results are in agreement with *in vivo* and *in vitro* experiments conducted on Pt@Alg in this study.

4. Conclusion

Cancer is on the front line of mortality and one of the economical burdens, worldwide. In this study, Pt@Alg nanoparticles were prepared to sensitize of cancer cells to X-ray irradiation. Successfully-Characterized nanoparticles manifested biocompatibility while enhancing the X-ray therapeutic effect on the 4 T1 cell line. Malignant cell radiosensitization benefits from the fact that intracellular ROS level is multiplied in contrast to the irradiated-only group. Regarding the results obtained from *in vivo* studies, the importance of radiosensitizers can be emphasized. Tumor growth was significantly suppressed in tumor-bearing mice co-administered with X-ray and radiosensitizer which was further confirmed by histopathological features of resected tumors.

Ethical considerations

This study was approved by the Ethics Committee of Erciyes University, and the study participants signed an informed consent.

CRediT authorship contribution statement

Hamid Rashidzadeh: Investigation, Software, Writing – original draft. **Farzad Seidi:** Methodology, Software, Resources. **Mohammadreza Ghaffarlou:** Investigation, Software, Formal analysis. **Marziyeh Salehiabar:** Methodology, Software, Formal analysis, Investigation. **Jalil Charmi:** Investigation, Software. **Kadir Yaray:** Investigation, Methodology. **Hamed Nosrati:** Conceptualization, Methodology, Software, Formal analysis, Investigation, Writing – review & editing. **Yavuz Nuri Ertas:** Resources, Software.

Declaration of competing interest

The authors declare no competing interests.

Data availability

The raw/processed data required to reproduce these findings cannot be shared at this time as the data also forms part of an ongoing study.

Acknowledgments

We gratefully acknowledge the Nanjing Forestry University. Y.N. Ertas acknowledges funding support from the 2232 International Fellowship for Outstanding Researchers Program of The Scientific and Technological Research Council of Türkiye (TÜBİTAK, Project No: 118C346).

References

[1] W.H. Organization. https://www.who.int/news-room/fact-sheets/detail/cancer. Accessed 3 February 2022.
[2] F. Bray, J. Ferlay, I. Soerjomataram, R.L. Siegel, L.A. Torre, A. Jemal, Global cancer statistics 2018: GLOBOCAN estimates of incidence and mortality worldwide for 36 cancers in 185 countries, CA Cancer J. Clin. 68 (6) (2018) 394–424.

[3] D.P. Budh, A. Sapra, Cancer Breast Screening, StatPearls Publishing, Treasure Island, FL, USA, 2021.
[4] Z. Momenimovahed, H. Salehiniya, Epidemiological characteristics of and risk factors for breast cancer in the world, Breast Cancer 11 (2019) 151.
[5] A.G. Waks, E.P. Winer, Breast cancer treatment: a review, JAMA 321 (3) (2019) 288–300.
[6] J. Sia, R. Szmyd, E. Hau, H.E. Gee, Molecular mechanisms of radiation-induced cancer cell death: a primer, Front.CellDev.Biol. 8 (2020).
[7] F. Abhari, J. Charmi, H. Rezaeejam, Z. Karimimoghaddam, H. Nosrati, H. Danafar, A. Farajollahi, Folic acid modified bismuth sulfide and gold heterodimers for enhancing radiosensitization of mice tumors to X-ray radiation, ACS Sustain. Chem. Eng. 8 (13) (2020) 5260–5269.
[8] A.A. Kirkham, R.I. Beaudry, D.I. Paterson, J.R. Mackey, M.J. Haykowsky, Curing breast cancer and killing the heart: a novel model to explain elevated cardiovascular disease and mortality risk among women with early stage breast cancer, Prog. Cardiovasc. Dis. 62 (2) (2019) 116–126.
[9] J. Wei, L. Meng, X. Hou, C. Qu, B. Wang, Y. Xin, X. Jiang, Radiation-induced skin reactions: mechanism and treatment, Cancer Manag. Res. 11 (2019) 167–177.
[10] L. Gong, Y. Zhang, C. Liu, M. Zhang, S. Han, Application of radiosensitizers in cancer radiotherapy, Int. J. Nanomedicine 16 (2021) 1083–1102.
[11] H. Wang, X. Mu, H. He, X.-D. Zhang, Cancer radiosensitizers, Trends Pharmacol. Sci. 39 (1) (2018) 24–48.
[12] M. Salehiabar, M. Ghaffarlou, A. Mohammadi, N. Mousazadeh, H. Rahimi, F. Abhari, H. Rashidzadeh, L. Nasehi, H. Rezaeejam, M. Barsbay, Y.N. Ertas, H. Nosrati, T. Kavetskyy, H. Danafar, Targeted CuFe2O4 hybrid nanoradiosensitizers for synchronous chemoradiotherapy, J. Control. Release 353 (2023) 850–863.
[13] Y. Zhang, X. Han, Y. Liu, S. Wang, X. Han, C. Cheng, Research progress on nano-sensitizers for enhancing effects of radiotherapy, Mater. Adv. 3 (2022) 3709–3725.
[14] Y. Li, K.H. Yun, H. Lee, S.H. Goh, Y.G. Suh, Y. Choi, Porous platinum nanoparticles as a high-Z and oxygen generating nanozyme for enhanced radiotherapy in vivo, Biomaterials 197 (2019) 12–19.
[15] W. Yang, H. Veroniaina, X. Qi, P. Chen, F. Li, P.C. Ke, Soft and condensed nanoparticles and nanoformulations for cancer drug delivery and repurpose, Adv. Ther. 3 (1) (2020), 1900102.
[16] H. Nosrati, F. Seidi, A. Hosseinmirzaei, N. Mousazadeh, A. Mohammadi, M. Ghaffarlou, H. Danafar, J. Conde, A. Sharafi, Prodrug polymeric nanoconjugates encapsulating gold nanoparticles for enhanced X-ray radiation therapy in breast cancer, Adv.Healthc.Mater. 11 (3) (2022), 2102321.
[17] D.M. Roquero, A. Othman, A. Melman, E. Katz, Iron (III)-cross-linked alginate hydrogels: a critical review, Mater. Adv. 3 (2022) 1849–1873.
[18] S. Maity, P. Mukhopadhyay, P.P. Kundu, A.S. Chakraborti, Alginate coated chitosan core-shell nanoparticles for efficient oral delivery of naringenin in diabetic animals—an in vitro and in vivo approach, Carbohydr. Polym. 170 (2017) 124–132.
[19] J. Castelló, M. Gallardo, M.A. Busquets, J. Estelrich, Chitosan (or alginate)-coated iron oxide nanoparticles: a comparative study, Colloids Surf. A Physicochem. Eng. Asp. 468 (2015) 151–158.
[20] X. Zhao, Q. Li, X. Ma, Z. Xiong, F. Quan, Y. Xia, Alginate fibers embedded with silver nanoparticles as efficient catalysts for reduction of 4-nitrophenol, RSC Adv. 5 (61) (2015) 49534–49540.
[21] S. Lee, C. Yim, S. Jeon, Direct synthesis of platinum nanodots in ZIF-8/Fe 3 O 4 core–shell hybrid nanoparticles, RSC Adv. 7 (50) (2017) 31239–31243.
[22] P. Rani, P. Pal, J.P. Panday, S. Mishra, G. Sen, Alginic acid derivatives: synthesis, characterization and application in wastewater treatment, J. Polym. Environ. 27 (12) (2019) 2769–2783.
[23] S.-H. Liao, C.-H. Liu, B.P. Bastakoti, N. Suzuki, Y. Chang, Y. Yamauchi, F.-H. Lin, K. C. Wu, Functionalized magnetic iron oxide/alginate core-shell nanoparticles for targeting hyperthermia, Int. J. Nanomedicine 10 (2015) 3315.
[24] C. Dablemont, P. Lang, C. Mangeney, J.-Y. Piquemal, V. Petkov, F. Herbst, G. Viau, FTIR and XPS study of pt nanoparticle functionalization and interaction with alumina, Langmuir 24 (11) (2008) 5832–5841.
[25] Y. Zhang, D. Zheng, S. Talaei, M. Abasi, Albumin stabilized Pt nanoparticles as radiosensitizer for sensitization of breast cancer cells under X-ray radiation therapy, Inorg. Chem. Commun. 140 (2022), 109423.
[26] C.M. Sayes, K.L. Reed, D.B. Warheit, Assessing toxicity of fine and nanoparticles: comparing in vitro measurements to in vivo pulmonary toxicity profiles, Toxicol. Sci. 97 (1) (2007) 163–180.
[27] J.C. Stockert, R.W. Horobin, L.L. Colombo, A. Blázquez-Castro, Tetrazolium salts and formazan products in cell biology: viability assessment, fluorescence imaging, and labeling perspectives, Acta Histochem. 120 (3) (2018) 159–167.
[28] M. Safdar, M. Ozaslan, R.A. Khailany, S. Latif, Y. Junejo, M. Saeed, M.S. Al-Attar, B. O. Kanabe, Synthesis, characterization and applications of a novel platinum-based nanoparticles: catalytic, antibacterial and cytotoxic studies, J. Inorg. Organomet. Polym. Mater. 30 (7) (2020) 2430–2439.
[29] J.C. Mohan, G. Praveen, K. Chennazhi, R. Jayakumar, S. Nair, Functionalised gold nanoparticles for selective induction of in vitro apoptosis among human cancer cell lines, J. Exp. Nanosci. 8 (1) (2013) 32–45.
[30] Q. Chen, Y. Luo, W. Du, Z. Liu, S. Zhang, J. Yang, H. Yao, T. Liu, M. Ma, H. Chen, Clearable theranostic platform with a pH-independent chemodynamic therapy enhancement strategy for synergetic photothermal tumor therapy, ACS Appl. Mater. Interfaces 11 (20) (2019) 18133–18144.
[31] N. Ma, Y.-W. Jiang, X. Zhang, H. Wu, J.N. Myers, P. Liu, H. Jin, N. Gu, N. He, F.-G. Wu, Z. Chen, Enhanced radiosensitization of gold nanospikes via hyperthermia in combined cancer radiation and photothermal therapy, ACS Appl. Mater. Interfaces 8 (42) (2016) 28480–28494.
[32] B. Perillo, M. Di Donato, A. Pezone, E. Di Zazzo, P. Giovannelli, G. Galasso, G. Castoria, A. Migliaccio, ROS in cancer therapy: the bright side of the moon, Exp. Mol. Med. 52 (2) (2020) 192–203.
[33] F. Daneshvar, F. Salehi, M. Karimi, R.D. Vais, M. Mosleh-Shirazi, N. Sattarahmady, Combined X-ray radiotherapy and laser photothermal therapy of melanoma cancer cells using dual-sensitization of platinum nanoparticles, J. Photochem. Photobiol. B Biol. 203 (2020), 111737.
[34] W. Jiang Z. Zhang M. Ye S. Pan G. Huang T. Chen X. Zhu , Morphology-Directed Radiosensitization of Mose2 Nanoplatforms for Promoting Cervical Cancer Radiotherapy.
[35] D. Rothley, Disparities in the Use of Radiation Therapy for Postlumpectomy Breast Cancer, Walden University, 2021.
[36] Q. Zhang, J. Liu, N. Ao, H. Yu, Y. Peng, L. Ou, S. Zhang, Secondary cancer risk after radiation therapy for breast cancer with different radiotherapy techniques, Sci. Rep. 10 (1) (2020) 1220.
[37] Q. Zhu, Y.M. Kirova, L. Cao, A. Arsene-Henry, J. Chen, Cardiotoxicity associated with radiotherapy in breast cancer: a question-based review with current literatures, Cancer Treat. Rev. 68 (2018) 9–15.
[38] A. Rajaee, S. Wang, L. Zhao, D. Wang, Y. Liu, J. Wang, K. Ying, Multifunction bismuth gadolinium oxide nanoparticles as radiosensitizer in radiation therapy and imaging, Phys. Med. Biol. 64 (19) (2019), 195007.
[39] J. Zhang, Y. Liu, X. Wang, J. Du, K. Song, B. Li, H. Chang, R. Ouyang, Y. Miao, Y. Sun, Y. Li, Nanozyme-incorporated biodegradable bismuth mesoporous radiosensitizer for tumor microenvironment-modulated hypoxic tumor thermoradiotherapy, ACS Appl. Mater. Interfaces 12 (52) (2020) 57768–57781.